

A new Böhm-Vitense gap in the temperature range 5560 to 5610 K in the Main Sequence [★] ^{★★}

V.V. Kovtyukh¹, C. Soubiran², and S.I. Belik¹

¹ Astronomical Observatory of Odessa National University and Isaac Newton Institute of Chile, Shevchenko Park, 65014, Odessa, Ukraine

² Observatoire Aquitain des Sciences de l'Univers, CNRS UMR 5804, BP 89, 33270 Floirac, France

Received 10 June 2004 / Accepted 20 July 2004

Abstract. Highly precise temperatures ($\sigma = 10 - 15$ K) have been determined from line depth ratios for a set of 248 F-K field dwarfs of about solar metallicity ($-0.5 < [\text{Fe}/\text{H}] < +0.4$), based on high resolution ($R=42\,000$), high S/N echelle spectra. A new gap has been discovered in the distribution of stars on the Main Sequence in the temperature range 5560 to 5610 K. This gap coincides with a jump in the microturbulent velocity V_t and the well-known Li depression near 5600 K in field dwarfs and open clusters. As the principal cause of the observed discontinuities in stellar properties we propose the penetration of the convective zone into the inner layers of stars slightly less massive than the Sun and related to it, a change in the temperature gradient.

Key words. Stars: fundamental parameters – stars: convection – H-R diagram

1. Introduction

Of the fundamental stellar parameters, effective temperature (T_{eff}) is the most crucial to obtain accurate abundances. There exists a multitude of methods to determine T_{eff} , among which we have chosen the line depth ratios. This method has the advantage of being independent of interstellar reddening, spectral resolution and rotational and microturbulence broadening. In a previous paper (Kovtyukh et al. 2003) we presented high precision temperatures for 181 F-K dwarfs by this method. We have noticed a gap in the temperature range 5560 to 5610 K ($B - V \sim 0.70$ for about solar metallicity) that we investigate in this paper.

Color gaps are known to exist in open clusters. For example, high-precision astrometry and photometry of the Hyades reveal two gaps along the clusters Main Sequence (MS), near $B - V \sim 0.38$ and ~ 0.48 mag (de Bruijne, Hoogerwerf & de Zeeuw 2000; 2001). Rachford & Canterna (2000) describe them in several other clusters. Among field stars, the existence of such gaps is still matter of debate (e.g., Böhm-Vitense & Canterna 1974; Mazzei & Pigatto

1988; Simon & Landsman 1997). Newberg & Yanny (1998) have used *Hipparcos* high-precision parallaxes, V and $B - V$, to construct the H-R diagram of nearby stars (primarily field stars, although their sample may contain cluster stars). They only found evidence for a gap at $B - V \sim 0.25$ in the MS.

The explanations for gaps range from the onset of convection in the stellar envelope (Böhm-Vitense & Canterna 1974) to peculiarities in the Balmer jump and Balmer lines as suggested by Mermilliod (1976). Ulrich (1971a; 1971b) speculated that gaps in young clusters might be produced by the presence of ^3He isotopes that halt gravitational contraction 1...2 mag above the MS. While Mermilliod's gaps occur among B stars, Böhm-Vitense & Canterna's (and also Ulrich's) gaps are found among less massive stars. Note that the standard stellar models do not show any peculiar change of slope in the T_{eff} versus mass relation along the MS. Böhm-Vitense (1970) was the first to realize that a gap in the distribution of colors may develop when the atmosphere changes from purely radiative to convective in the deep layers at T_{eff} cooler of ~ 7500 K. There are two possible ways in which convection might alter T_{eff} : (a) either because the convective temperature gradient is steeper than radiative (Böhm-Vitense 1970); or (b) because convection causes photospheric granulation with associated temperature inhomogeneities (Nelson 1980; Böhm-Vitense 1982).

In order to investigate the existence of gap in the MS, we have increased our initial sample to 248 stars, with

Send offprint requests to: V.V. Kovtyukh,
e-mail: val@deneb.odessa.ua

[★] Based on spectra collected with the ELODIE spectrograph at the 1.93-m telescope of the Observatoire de Haute Provence (France).

^{★★} Full Table 1 is only available in electronic form at <http://www.edpsciences.org>

T_{eff} ranging from 4000 to 6150 K and absolute magnitudes M_V from 3.02 to 7.41. In Sect. 2, we briefly describe our dataset and the method of line depth ratios. In Sect. 3, we confirm the existence of a gap in the temperature range 5560 to 5610 K and we show that it is not correlated with $[\text{Fe}/\text{H}]$ but with the microturbulence velocity V_t . Also we discuss the possible coincidence of this gap with the Li depression observed in field stars and open clusters.

2. Data reduction and the derivation of atmospheric parameters

The spectra used in this paper were extracted from the most recent version of the library of stellar spectra collected with the ELODIE echelle spectrograph at the Observatoire de Haute-Provence by Soubiran et al. (1998) and Prugniel & Soubiran (2001). The description of the instrument mounted on the 1.93 m telescope can be found in Baranne et al (1996).

Most of the stars have accurate *Hipparcos* parallaxes enabling us to determine their absolute magnitudes M_V that range from 3.016 (HD 209965, F8V) to 7.410 (HD 29697, K3V). HD 209965 however has the most uncertain absolute magnitude due to a relative error in parallax of 18% (all the others have relative errors lower than 11%). Two stars that are not part of the *Hipparcos* catalogue had their absolute magnitudes estimated by the TGMET method introduced by Katz et al. (1998): HD 171304 ($M_V=4.238$), HD 186039 ($M_V=4.026$).

The spectral range of the spectra is 4400–6800 Å and the resolution is $R=42\,000$. The signal to noise ratio (S/N) of the spectra range from 40 to 680, with the large majority having $S/N > 100$. Spectrum extraction, wavelength calibration and radial velocity measurement were performed at the telescope with the on-line data reduction software while straightening of the orders, removing of cosmic ray hits, bad pixels and telluric lines were performed as described in Katz et al (1998). Further processing of the spectra (continuum placement, measuring equivalent widths, etc.) was carried out by us using the DECH20 software (Galazutdinov 1992). Equivalent widths and depths R_λ of lines were measured manually by means of a Gaussian fitting. The Gaussian height was taken as a measure of the line depth. This method produces line depth values that agree with the parabola technique used by Gray (1994).

The key to our analysis of the stellar spectra is the line-depth ratio technique, pioneered by Gray (1994) and successively improved by our group. This technique allows the determination of T_{eff} with an exceptional precision. It relies on the ratio of the central depths of two lines that have very different functional dependences on T_{eff} . The method is independent of the interstellar reddening and only marginally dependent on individual characteristics of stars, such as rotation, microturbulence and metallicity.

Briefly, a set of 105 line ratio – T_{eff} relations was obtained in Kovtyukh et al. (2003), with the mean random error of a single calibration being 60–70 K (40–45 K in

most cases and 90–95 K in the least accurate cases). The use of ~ 70 –100 calibrations per spectrum reduces the uncertainty to 5–7 K. These 105 relations use 92 lines, 45 with low ($\chi < 2.77$ eV) and 47 with high ($\chi > 4.08$ eV) excitation potentials, and have been calibrated with the 45 reference stars in common with Alonso et al. (1996), Blackwell & Lynas-Gray (1998) and di Benedetto (1998). The zero-point of the temperature scale was directly adjusted to the Sun ($T_{\text{eff}} = 5777$ K is adopted for the Sun), based on 11 solar reflection spectra taken with ELODIE, leading to an uncertainty in the zero-point of about 1 K. The application range for the calibrations is $-0.5 < [\text{Fe}/\text{H}] < +0.4$.

In the present study we add 82 new spectra to the 2003 sample, increasing the total number of dwarfs with precisely determined T_{eff} to 248 (see Table 1). In Table 1 we give the mean T_{eff} , the number of calibrations used (N), the errors of the mean σ , $\log g$, V_t , $[\text{Fe}/\text{H}]$, M_V and $B - V$ from *Tycho2* (transformed into Johnson). For the majority of stars we get an error which is smaller than 10 K.

Accurate $[\text{Fe}/\text{H}]$, $\log g$ and V_t have been determined as well. The iron abundance was determined from an LTE analysis of equivalent widths of FeI and FeII lines using the WIDTH9 code and the atmosphere models by Kurucz (1993). Appropriate models for each star were derived by means of standard interpolation through T_{eff} and $\log g$.

Microturbulent velocities V_t were determined by forcing abundances obtained from individual FeI lines to be independent of equivalent width. The value of V_t is very sensitive to the adopted T_{eff} . The small uncertainty of 0.1–0.2 km s^{-1} is the result of our T_{eff} estimates being accurate to 10–20 K.

Surface gravities $\log g$ were derived from the ionization balance between FeI and FeII.

The abundance of iron relative to solar $[\text{Fe}/\text{H}] = \log(\text{Fe}/\text{H})_* - \log(\text{Fe}/\text{H})_\odot$ was adopted as the metallicity parameter of a star and was obtained from FeI lines. Note that the solar metallicity from our analysis is $[\text{Fe}/\text{H}] = 0.05$ (Table 1). This non-zero value results from the lower resolution of our spectra ($R = 42\,000$) compared to the resolution of the Solar Spectrum Atlas ($R \sim 600\,000$) which is usually used for solar oscillator strengths and $[\text{Fe}/\text{H}]_\odot$ determinations. For some stars the atmospheric parameters have been previously reported in Mishenina et al. (2004).

3. The gap

Fig. 1 shows the resulting temperature versus absolute magnitude for our 248 field dwarfs. A number of turn-offs and a well-defined MS can be seen. The latter shows a clear gap between $T_{\text{eff}} = 5560$ and 5610 K ($B - V \sim 0.70$ mag for about solar metallicity) and $M_V = 5.0$ –5.5 mag, which corresponds to a mass of about 0.90–0.95 M_\odot . This gap has been tentatively identified in Hyades by De Bruijne, Hoogerwerf & de Zeeuw (2000, 2001), although it is less prominent than the other two gaps in this cluster (since

Table 1. Program stars.

Star	T_{eff} , K	N	σ , K	$\log g$	V_t , km s^{-1}	[Fe/H]	M_V	(B-V)	Remarks
HD 1562	5828	97	5.8	4.0	1.2	-0.27	5.007	0.589	
HD 1835	5790	68	5.5	4.4	0.9	0.20	4.843	0.644	
HD 3765	5079	87	4.7	4.3	1.1	0.06	6.155	0.953	
HD 4307	5889	91	5.0	4.0	1.1	-0.13	3.637	0.583	
HD 4614	5965	69	6.4	4.4	1.2	-0.19	4.591	0.542	

Hyades has $[\text{Fe}/\text{H}] = +0.15$, this leads to a shift of the $(B - V)_{\text{gap}}$ to 0.75–0.80).

The gap (near $(B - V) \sim 0.70$) is not clearly seen in the $(B - V) - M_V$ diagram for our sample of field stars, because the $(B - V)$ parameter is very sensitive to interstellar reddening, metallicity and macroturbulence.

What is the probability that the gap is due to statistical uncertainty in the star counts? The histogram appears to be a smoothly increasing function between $T_{\text{eff}} = 4900$ and 5900 (Fig. 2a). Approximating by a quadratic polynomial, we get a dispersion in the distribution of about ± 3.2 (point (5585,0) included) or ± 2.0 (point (5585,0) excluded). This predicts 12 stars in the region of the gap (centered on $T_{\text{eff}} = 5585$ K). No star in the gap requires a minimum of 4σ deviation, which translates into the probability that the gap is real as high as 0.999.

Note that one star (excluded from Table 1) does fall into the gap. HD 13974 is a G0V spectroscopic binary, with $T_{\text{eff}} = 5590 \pm 12.9$ and $[\text{Fe}/\text{H}] = -0.46$. The value of $\log g = 3.9$ for this star is more typical of a subgiant, as well as $M_V = 4.697$. We therefore conclude it is not a dwarf. Also quite possibly the spectrum of the secondary component distorts our measurements of the lines of the primary component and therefore affects the derived T_{eff} .

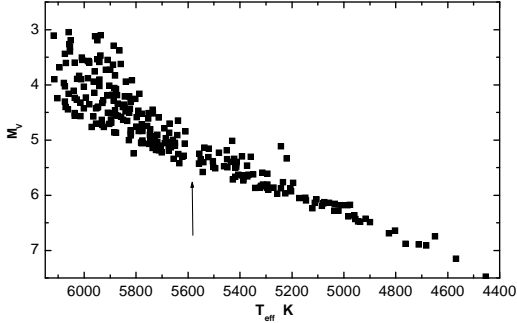


Fig. 1. Temperature-absolute magnitude diagram for 248 field dwarfs. The errors in the temperature are less than the symbol size. An arrow indicates the gap, which may be caused by the sudden changes in the properties of atmospheric convection near $T_{\text{eff}} = 5560$ K.

It is reasonable to assume that microturbulence is driven by convection and therefore one might expect a discontinuous behavior of V_t across the gap. Indeed, as seen from Fig. 2b, V_t experiences a jump at the position of the gap. On the hot side, V_t declines from 1.3 km s^{-1}

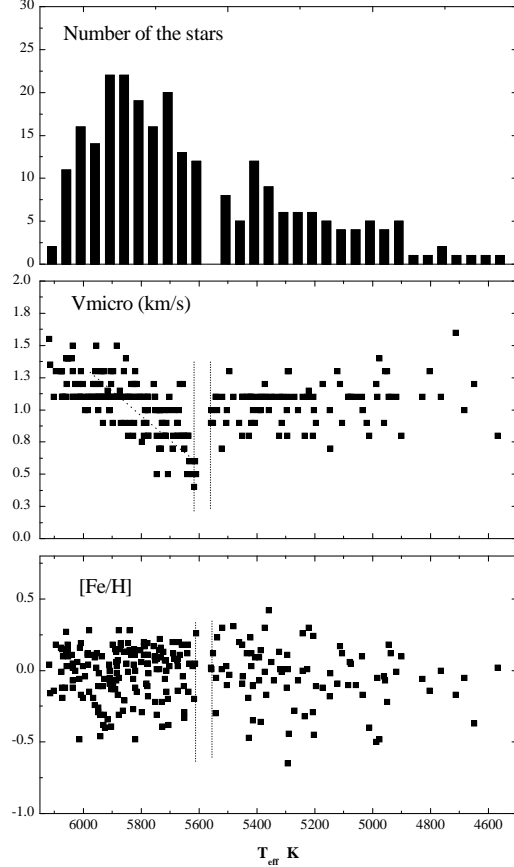


Fig. 2. (a)– A histogram of field dwarf distribution with temperature. The bin size is 50 K, starting from the minimum temperature of 4510 K; (b)– Microturbulent velocity versus T_{eff} ; (c)– Iron abundance vs. T_{eff} .

at $T_{\text{eff}} = 6000$ K to 0.6 km s^{-1} at 5560 K. On the cool side, V_t is nearly constant at 1.0 km s^{-1} . This test has not been carried out before and may be an indirect confirmation of the convection hypothesis. It is very important to note that this jump remains even if we decrease T_{eff} by 50 K for the stars located near the hot boundary of the gap. Therefore we conclude that this jump is real.

To demonstrate that there is no systematic effect in our T_{eff} or V_t determination, we plot the derived metallicities versus T_{eff} in Fig. 2c. There is no trend of $[\text{Fe}/\text{H}]$ with T_{eff} which confirms the robustness of our atmospheric analysis. Also, it shows that our sample is very uniform

in metallicity, $[\text{Fe}/\text{H}]$ spanning the full interval at all temperatures.

The dwarfs in our sample have various ages, and they likely evolve within the MS. Why then the position of the gap does remain independent of the stars' ages and their evolutionary stages? One possible solution is that. The structure of the outer parts of the convective zones is independent of small luminosity changes during the MS stage, but depends mainly upon the T_{eff} . Therefore, stars in the vicinity of the gap should experience the color and T_{eff} jumps, placing them outside the gap. Thus, we can consider these jumps as a result of the sudden rebuilding of the outer convective zone structure that change the color and T_{eff} of the stars.

3.1. The possible lithium – gap connection

The gap is located near the hot edge of the well-studied lithium depression in the field dwarfs at $T_{\text{eff}} < 5600$, where lithium is depleted by 2 or more orders of magnitude (see, for example, Chen et al. 2001; Ryan 2000). The dwarfs located on the left of the blue side of the gap show a large spread in lithium abundance, with values A_{Li} ranging from less than 1.0 to 3.0 dex. In contrast, stars located on the right of red side show low values of A_{Li} , reflecting the dilution effects in this spectral region.

The surface abundance of Li should in principle be a function of T_{eff} , age, metallicity and somewhat poorly explored physical processes like convection, rotation, stellar wind, etc. Thus, by measuring Li in stars with nearly solar metallicity, crucial information about the convection in stars of different ages can be obtained. The level of dilution of lithium depends on the level of convection in these stars.

Li depression is observed in field stars and old clusters such as Coma, Hyades, M 67 but not in the younger ones like Pleiades and Alpha Per. The location of Li depression is also age-dependent: in the Hyades (625 Myr) it occurs at $T_{\text{eff}} \sim 5400$ K (Boesgaard & King 2002), in NGC 752 (1.7 Gyr) at $T_{\text{eff}} \sim 5600$ K, and in M 67 (5 Gyr) at $T_{\text{eff}} \sim 5700$ K (Ryan 2000). Only stars that have shallow convection regions will show Li enrichment - when a star has a large convective region, the Li is diluted beyond detection. Cool dwarfs ($T_{\text{eff}} < 5600$ K) usually show lower Li abundance compared to hot ones. Only a few cool dwarfs are known to have a high Li content (Chen et al. 2001).

It is clear that the sudden decline in A_{Li} near the temperature gap is directly associated with a rapid increase in thickness of the convective envelope in such regions (e.g. Cayrel, Cayrel de Strobel & Campbell 1984; Chen et al. 2001). Most of the stars with high Li abundance present an undeveloped convective zone, whereas stars with low Li abundance show a developed convective zone.

Israelian et al. (2004) find that lithium abundances of planet host stars with T_{eff} between 5850 and 6350 K are similar to those in the Chen et al. (2001) comparison sample, while at lower T_{eff} , in the range 5600 – 5850

K, the planet host stars show on average lower lithium abundances than stars in the comparison sample. This temperature range is where anomalous behavior of the microturbulence velocity is observed (Fig. 2b).

4. Summary

To investigate the fine structure in the distribution of stars on the MS, we have determined precise T_{eff} for a sample of 248 field F, G and K stars with accurate *Hipparcos* parallaxes and near-solar metallicity $-0.5 < [\text{Fe}/\text{H}] < 0.4$. We have identified a new Böhm-Vitense gap in the MS between 5560 and 5610 K, with a confidence better than 99.9%. This gap possibly coincides with the Li depression seen in open clusters and field stars. The most likely explanation for the gap is the sudden change in the properties of atmospheric convection.

Our analysis suggests that the theoretical models of convection in solar-type stars need to be improved.

Acknowledgements. V.K. wants to thank the staff of Observatoire de Bordeaux for the kind hospitality during his stay there. In addition, V.K. would like to thank Prof. G.S. Bisnovatyi-Kogan and Dr. N.I. Gorlova for many useful discussions about stellar physics. The authors are grateful to the referee, Dr. B.A. Twarog, for helpful comments and suggestions which have certainly improved the final version of this paper.

References

- Alonso, A., Arribas, S., & Martínez-Roger, C. 1996, A&ASS 117, 227
- Baranne, A., Queloz, D., Mayor, M., et al. 1996, A&AS, 119, 373
- Blackwell, D.E. & Lynas-Gray, A.E. 1998, A&ASS 129, 505
- Boesgaard, A.M. & King J.R., 2002, A&A, 565, 587
- Böhm-Vitense, E. 1970, A&A, 8, 283
- Böhm-Vitense, E. 1982, ApJ, 255, 191
- Böhm-Vitense, E., & Canterna, R. 1974, ApJ, 194, 629
- Cayrel, R., Cayrel de Strobel, G., & Campbell, B., 1984, ApJ, 283, 205
- Chen Y.Q., Nissen P.E., Benoti T., Zhao G., 2001, A&A, 371, 943
- de Bruijne, J.H.J., Hoogerwerf, R., & de Zeeuw, P.T. 2000, ApJ, 544, L65
- de Bruijne, J.H.J., Hoogerwerf, R., & de Zeeuw, P.T. 2001, A&A 367, 111
- di Benedetto, G.P. 1998, A&A 339, 858
- Galazutdinov G.A., 1992, Preprint SAO RAS, n92
- Gray D., 1994, PASP 106, 1248
- Israelian, G., Santos, N.C., Mayor, M. & Rebolo, R. 2004, A&A, 414, 601
- Katz, D., Soubiran, C., Cayrel, R., Adda, M. & Cautain, R. 1998, A&A, 338, 151
- Kovtyukh, V.V., Soubiran, C., Belik, S.I., & Gorlova N.I. 2003, A&A, 411, 559
- Kurucz R.L., 1993, CD ROM n13
- Mazzei, P., & Pigatto, L. 1988, A&A, 193, 148
- Mermilliod, J.-C. 1976, A&A, 53, 289
- Mishenina, T.V., Soubiran, C., Kovtyukh, V.V., Korotin, S.A. 2004, A&A, 418, 551

- Nelson, G.D. 1980, ApJ, 238, 659
Newberg, H.J. & Yanny, B. 1998, ApJ, 499, L57
Prugniel, P. & Soubiran, C., 2001, A&A 369, 1048
Rachford, B.J., & Canterna, R. 2000, AJ, 119, 1296
Ryan, S., 2000, MNRAS, 316, L35
Simon, T., & Landsman, W.B. 1997, ApJ, 484, 360
Soubiran, C., Katz, D. & Cayrel, R., 1998, A&AS, 133, 221
Ulrich, R.K. 1971a, ApJ, 165, L95
Ulrich, R.K. 1971b, ApJ, 168, 57

Table 1. Program stars.

Star	T_{eff} , K	N	σ , K	$\log g$	V_t , km s^{-1}	[Fe/H]	M_V	(B-V)	Remarks
HD001562	5828	97	5.8	4.0	1.2	-0.27	5.007	0.589	
HD001835	5790	68	5.5	4.4	0.9	0.20	4.843	0.644	
HD003765	5079	87	4.7	4.3	1.1	0.06	6.155	0.953	
HD004307	5889	91	5.0	4.0	1.1	-0.13	3.637	0.583	
HD004614	5965	69	6.4	4.4	1.2	-0.19	4.591	0.542	
HD004635	5129	94	5.5	4.4	0.9	0.12	6.069	0.916	
HD005294	5779	86	6.6	4.4	1.1	-0.11	5.067	0.602	
HD006715	5652	97	6.7	4.5	0.8	-0.11	5.062	0.665	
HD007924	5153	82	5.8	4.4	1.0	-0.18	6.029	0.820	
HD008574	6028	61	6.7	4.2	1.2	0.00	3.909	0.527	
HD008648	5790	59	7.2	4.2	1.1	0.17	4.411	0.626	
HD009826	6074	44	13.1	4.0	1.3	0.15	3.454	0.501	
HD010086	5686	96	4.4	4.5	1.0	0.08	4.955	0.657	
HD010145	5673	96	4.2	4.3	0.8	0.08	4.881	0.667	
HD010307	5881	94	4.0	4.3	1.1	0.07	4.450	0.583	
HD010476	5242	69	3.2	4.3	1.1	0.00	5.874	0.835	
HD010700	5427	83	12.1	4.4	0.8	-0.47	5.678	0.727	
HD010780	5407	95	4.0	4.4	0.9	0.09	5.623	0.778	
HD011007	5980	84	7.4	4.0	1.1	-0.15	3.611	0.525	
HD012051	5470	95	4.9	4.3	1.1	0.18	5.190	0.766	
HD012846	5751	80	6.0	4.5	1.0	-0.22	5.072	0.618	
HD013507	5714	91	5.4	4.5	0.8	0.07	5.103	0.637	
HD013579	5253	83	8.4	4.3	1.15	0.30	5.260	0.907	
HD013825	5705	96	5.5	4.2	1.0	0.20	4.691	0.671	
HD014374	5449	77	4.6	4.3	1.1	-0.04	5.519	0.748	
HD015335	5937	84	6.6	3.95	1.1	-0.11	3.460	0.549	
HD017674	5909	58	8.7	4.0	1.1	-0.09	4.198	0.549	
HD017925	5225	87	5.0	4.4	1.1	0.01	5.954	0.865	
HD018632	5141	87	5.8	4.3	1.2	0.17	6.103	0.928	
HD018803	5659	95	3.5	4.3	0.8	0.18	4.993	0.688	
HD019019	6063	56	7.2	4.0	1.1	-0.12	4.437	0.502	
HD019308	5844	95	5.4	4.3	1.1	0.13	4.223	0.615	
HD019373	5963	75	5.1	4.2	1.1	0.11	3.941	0.568	
HD019994	6055	56	10.0	4.0	1.4	0.15	3.320	0.530	
HD020165	5148	84	3.5	4.4	0.7	-0.02	6.074	0.887	
HD020630	5718	80	3.8	4.55	1.0	0.07	5.034	0.643	
HD022049	5084	84	5.9	4.4	1.1	-0.10	6.170	0.877	
HD022484	6037	60	3.6	4.1	1.1	0.02	3.607	0.532	
HD023050	5929	80	9.0	4.4	1.1	-0.31	4.342	0.548	
HD024040	5787	103	4.5	4.2	1.0	0.17	4.166	0.641	SB2 ?
HD024053	5723	93	3.7	4.4	0.8	0.13	5.173	0.665	
HD024206	5633	94	4.8	4.5	0.6	0.05	5.424	0.688	
HD024238	5015	80	10.5	4.0	1.2	-0.50	6.186	0.845	
HD024409	5748	99	5.3	4.5	0.5	0.01	4.888	0.651	
HD024496	5557	82	3.8	4.5	1.0	0.01	5.232	0.704	
HD025665	4970	71	5.9	4.2	0.9	-0.04	6.355	0.954	
HD025893	5387	80	5.2	4.6	1.0	0.14	5.546	0.823	
HD026913	5656	85	5.5	4.5	1.2	-0.04	5.342	0.638	
HD026923	5933	77	5.9	4.2	1.3	-0.10	4.689	0.545	
HD028005	5980	87	6.1	4.2	1.1	0.28	4.355	0.666	
HD028099	5778	85	5.2	4.3	1.2	0.17	4.758	0.663	
HD029150	5733	89	5.4	4.4	0.7	0.09	4.952	0.637	
HD029310	5852	89	7.7	4.2	1.4	0.13	4.399	0.555	
HD029645	6009	57	5.8	4.0	1.3	0.19	3.505	0.550	
HD029697	4454	40	11.4	4.5	1.1	0.01	7.410	1.115	
HD030495	5820	91	5.7	4.4	1.3	0.00	4.868	0.604	
HD030562	5859	87	6.8	4.05	1.3	0.13	3.656	0.603	
HD032147	4945	65	8.7	4.4	1.1	0.18	6.474	1.075	

Table 1 (Continued)

Star	T_{eff} , K	N	σ , K	$\log g$	V_t , km s^{-1}	[Fe/H]	M_V	(B-V)	Remarks
HD032850	5314	91	6.4	4.4	1.0	-0.12	5.837	0.785	
HD033632	6072	44	14.1	4.3	1.1	-0.19	4.413	0.493	
HD034411	5890	88	4.3	4.2	1.1	0.15	4.187	0.592	
HD036667	5949	58	10.3	4.1	1.2	-0.29	3.531	0.530	
HD037008	5038	82	8.9	4.2	0.8	-0.40	6.154	0.811	
HD037124	5651	80	9.9	4.5	0.7	-0.29	5.047	0.663	
HD038230	5241	92	6.3	4.6	0.8	-0.32	5.765	0.832	
HD038858	5776	81	6.7	4.3	1.1	-0.18	5.005	0.640	
HD039587	5955	71	6.1	4.3	1.5	0.02	4.712	0.560	
HD039833	5822	90	4.8	4.2	1.2	0.11	4.294	0.584	
HD040616	5881	89	10.0	4.0	1.1	-0.17	3.828	0.582	
HD040650	5994	74	5.7	4.3	1.0	-0.04	4.231	0.517	
HD041330	5904	77	5.5	4.1	1.2	-0.13	4.019	0.554	
HD041593	5312	92	3.3	4.3	1.1	0.01	5.808	0.804	
HD042618	5775	96	6.6	4.5	0.8	-0.02	5.040	0.600	
HD042807	5737	81	5.2	4.45	1.0	0.01	5.139	0.635	
HD043587	5927	81	4.4	4.1	1.3	-0.06	4.278	0.574	
HD043947	6001	82	7.1	4.3	1.1	-0.19	4.424	0.513	
HD045067	6058	61	4.6	4.0	1.2	0.03	3.284	0.515	
HD047127	5639	91	5.1	4.3	0.8	0.18	4.652	0.699	
HD047309	5791	95	3.9	4.35	0.8	0.11	4.467	0.623	
HD049385	6052	56	6.7	4.0	1.4	0.10	3.187	0.511	vsini= 7.5
HD050281	4712	56	8.5	3.9	1.6	-0.17	6.859	1.074	
HD050554	5977	77	5.8	4.1	1.1	-0.02	4.396	0.532	
HD051419	5746	94	8.3	4.3	0.8	-0.31	5.011	0.598	
HD051866	4939	82	5.6	4.2	1.1	-0.01	6.413	0.998	
HD054371	5666	89	5.0	4.3	1.2	0.11	5.134	0.674	
HD055575	5949	65	6.6	4.3	1.1	-0.26	4.415	0.543	
HD056515	5983	69	6.4	4.4	1.1	0.04	3.502	0.556	
HD058595	5707	87	8.3	4.6	0.5	-0.20	5.105	0.655	
HD059747	5137	87	4.4	4.2	1.3	-0.09	6.194	0.851	
HD061606	4956	83	4.6	4.4	1.3	-0.07	6.406	0.940	
HD062613	5541	90	6.4	4.4	1.1	-0.05	5.396	0.706	
HD063433	5702	89	5.6	4.5	1.1	0.03	5.216	0.646	
HD064815	5864	88	8.3	4.0	1.1	-0.28	3.373	0.596	
HD065874	5936	85	4.7	4.0	1.3	0.10	3.102	0.564	
HD066573	5819	86	11.6	4.6	1.1	-0.48	4.911	0.555	
HD068017	5651	100	9.0	4.4	0.8	-0.33	5.106	0.624	
HD068638	5430	90	6.3	4.4	1.1	-0.19	5.010	0.745	
HD070110	5958	84	6.3	4.1	1.3	0.10	3.127	0.570	
HD070923	5986	82	4.5	4.2	1.1	0.11	3.879	0.553	
HD071148	5850	88	5.1	4.2	1.1	0.05	4.635	0.588	
HD071640	5961	70	11.8	4.1	1.2	-0.24	4.148	0.477	uncertain Vr
HD072760	5349	91	3.8	4.1	1.1	0.06	5.627	0.772	
HD072905	5884	79	6.8	4.4	1.5	-0.02	4.862	0.581	
HD073226	5846	87	6.9	4.4	0.8	0.19	4.356	0.613	
HD073344	6060	37	6.8	4.1	1.1	0.13	4.171	0.519	
HD073668	5909	76	7.2	4.4	1.0	0.00	4.493	0.547	
HD074156	5986	56	7.2	4.2	1.0	0.12	3.575	0.535	
HD075302	5690	83	6.0	4.5	0.8	0.12	5.075	0.658	
HD075318	5450	78	5.8	4.4	0.8	-0.09	5.351	0.717	
HD075732	5373	97	9.7	4.3	1.1	0.30	5.459	0.862	
HD076151	5776	88	3.0	4.3	1.0	0.11	4.844	0.639	
HD076780	5761	87	5.0	4.2	1.0	0.16	5.005	0.646	
HD079555	4803	56	11.0	4.1	1.3	-0.14	6.583	1.012	
HD080536	5899	79	7.2	4.3	0.9	0.18	3.723	0.588	
HD082106	4827	76	6.0	4.1	1.1	-0.06	6.660	0.995	
HD082885	5545	85	8.1	4.3	1.1	0.30	5.154	0.758	
HD086728	5735	91	5.6	4.2	1.0	0.22	4.510	0.644	
HD088072	5778	82	5.0	4.3	1.1	0.05	4.696	0.640	

Table 1 (Continued)

Star	T_{eff} , K	N	σ , K	$\log g$	V_t , km s^{-1}	[Fe/H]	M_V	(B-V)	Remarks
HD088986	5840	91	6.0	4.2	0.9	0.14	3.942	0.598	
HD089251	5886	89	6.3	4.0	1.1	-0.07	3.289	0.571	
HD089269	5674	95	5.7	4.45	0.9	-0.14	5.084	0.656	
HD089389	6031	48	8.9	4.2	1.2	0.03	4.035	0.535	
HD090508	5858	68	9.1	4.4	0.9	-0.21	4.572	0.568	
HD091347	5923	75	7.4	4.4	1.1	-0.38	4.727	0.513	
HD095128	5887	89	3.8	4.3	1.1	0.06	4.289	0.586	
HD096094	5936	73	11.6	3.9	1.15	-0.34	3.724	0.543	
HD098630	6060	52	10.0	4.0	1.4	0.27	3.037	0.543	
HD099491	5509	96	8.6	4.3	1.1	0.31	5.249	0.779	
HD099505	5781	65	6.5	4.5	0.9	-0.09	5.033	0.608	
HD101177	5932	58	8.4	4.3	0.9	-0.11	4.453	0.590	
HD101206	4649	60	7.6	4.0	1.2	-0.37	6.726	0.990	
HD101227	5543	73	7.2	4.5	1.1	-0.30	5.590	0.661	
HD101501	5558	88	6.1	4.5	0.9	0.02	5.408	0.712	
HD102870	6055	48	6.8	4.0	1.4	0.18	3.412	0.521	
HD106116	5691	95	4.1	4.5	0.7	0.20	4.777	0.675	SB2 ?
HD106210	5718	90	6.1	4.5	0.8	-0.06	4.917	0.654	
HD106252	5878	62	7.6	4.2	1.1	-0.05	4.555	0.584	
HD107705	6040	56	7.8	4.2	1.4	0.11	4.093	0.515	
HD108954	6037	60	5.5	4.4	1.3	-0.07	4.507	0.520	
HD109358	5897	72	6.2	4.2	1.1	-0.13	4.633	0.557	
HD110833	5075	80	3.9	4.3	1.1	0.05	6.111	0.932	
HD110897	5925	68	12.3	4.2	1.1	-0.40	4.759	0.515	
HD112758	5203	83	8.4	4.1	1.0	-0.45	5.925	0.779	
HD114710	5954	71	6.8	4.3	1.1	0.12	4.433	0.548	
HD115383	6012	40	9.3	4.3	1.1	0.16	3.924	0.547	
HD116443	4976	83	9.9	4.0	1.4	-0.48	6.235	0.844	
HD117043	5610	98	4.7	4.45	0.5	0.26	4.854	0.726	
HD119802	4763	71	6.6	4.0	1.1	0.00	6.867	1.046	
HD122064	4937	84	8.1	4.5	1.1	0.12	6.445	1.041	
HD122120	4568	35	11.4	4.3	0.8	0.02	7.128	1.162	
HD124292	5535	89	4.0	4.5	0.7	0.01	5.302	0.723	
HD126053	5728	79	6.9	4.45	0.9	-0.22	5.029	0.602	
HD126512	5941	76	11.2	4.3	1.3	-0.50	3.921	0.535	
HD129499	5960	53	9.8	4.2	1.1	0.09	3.764	0.552	
HD130322	5418	85	5.4	4.55	0.9	0.03	5.669	0.756	
HD131977	4683	62	6.8	4.0	1.0	-0.05	6.857	1.101	
HD132142	5206	75	9.9	4.2	0.8	-0.29	5.863	0.788	
HD135204	5413	91	4.6	4.0	1.1	-0.11	5.387	0.739	
HD135599	5257	86	5.1	4.4	1.0	-0.07	5.949	0.811	
HD136923	5392	86	5.2	4.4	1.0	-0.07	5.634	0.786	
HD137107	6037	60	6.9	4.3	1.1	0.05	3.645	0.530	
HD139323	5204	90	7.7	4.6	1.1	0.24	5.891	0.947	
HD139341	5242	90	7.9	4.6	1.1	0.26	5.074	0.897	
HD140538	5675	100	3.5	4.5	0.9	0.07	5.032	0.647	
HD141004	5884	81	4.4	4.1	1.1	0.03	4.069	0.571	
HD143761	5865	81	11.1	4.3	0.8	-0.06	4.196	0.572	
HD144287	5414	93	5.7	4.5	1.1	-0.10	5.434	0.738	
HD144579	5294	89	10.3	4.1	1.3	-0.65	5.870	0.713	
HD145675	5406	98	12.1	4.3	1.0	0.42	5.310	0.870	
HD145729	6014	32	12.9	4.3	1.2	-0.06	4.328	0.506	
HD146233	5799	96	3.8	4.4	1.1	0.06	4.762	0.626	
HD149661	5294	90	3.2	4.5	1.1	0.01	5.807	0.830	
HD151541	5368	88	6.4	4.2	1.1	-0.17	5.624	0.755	
HD152391	5495	82	4.5	4.3	1.3	-0.03	5.505	0.728	
HD154345	5503	87	5.6	4.5	1.0	-0.10	5.482	0.706	
HD154931	5910	82	6.7	4.0	1.1	-0.05	3.563	0.572	
HD157089	5941	71	13.1	4.15	1.1	-0.46	4.026	0.526	

Table 1 (Continued)

Star	T_{eff} , K	N	σ , K	$\log g$	V_t , km s^{-1}	[Fe/H]	M_V	(B-V)	Remarks
HD157214	5784	85	9.5	4.4	0.75	-0.29	4.594	0.580	
HD158614	5641	98	3.6	4.6	0.5	0.12	4.231	0.693	
HD158633	5290	83	10.7	4.2	1.3	-0.44	5.887	0.751	
HD159062	5414	96	7.9	4.3	1.0	-0.35	5.471	0.711	
HD159222	5834	93	4.0	4.3	1.2	0.11	4.653	0.614	
HD159909	5749	93	5.6	4.3	0.7	0.14	4.462	0.646	
HD160346	4983	84	3.9	4.3	1.1	-0.05	6.347	0.955	
HD160933	5949	52	7.8	4.0	1.0	-0.11	3.199	0.553	
HD161098	5617	90	7.3	4.5	0.4	-0.20	5.287	0.624	
HD164651	5613	84	4.6	4.45	0.6	0.05	5.089	0.704	
HD164922	5392	96	6.0	4.3	1.1	0.09	5.296	0.796	
HD165173	5505	95	4.7	4.4	0.9	0.03	5.383	0.739	
HD165341	5314	92	4.4	4.4	0.9	-0.01	5.465	0.864	
HD165401	5877	85	8.5	4.3	1.1	-0.31	4.868	0.554	
HD165476	5845	90	5.9	4.1	1.1	-0.01	4.389	0.573	
HD165672	5871	89	6.2	4.4	0.9	0.19	4.569	0.614	
HD166620	5035	75	5.7	4.0	1.0	-0.17	6.141	0.876	
HD168009	5826	93	4.0	4.1	1.1	0.04	4.528	0.604	
HD170512	6078	43	9.4	4.3	1.3	0.16	3.971	0.550	
HD171067	5674	81	6.5	4.4	0.8	0.03	5.197	0.662	
HD171304	5871	89	4.9	4.1	1.1	0.18	4.238	0.610	
HD173701	5423	104	9.7	4.4	1.1	0.23	5.344	0.850	
HD174719	5637	86	7.5	4.55	0.8	-0.15	5.256	0.672	
HD175726	6036	26	15.1	4.4	1.5	-0.12	4.562	0.533	vsini= 13.5
HD176841	5841	92	6.2	4.3	1.1	0.28	4.481	0.627	
HD182488	5435	82	4.4	4.4	1.1	0.12	5.406	0.787	
HD183341	5911	85	3.9	4.3	1.0	0.04	4.207	0.572	
HD184385	5552	87	4.1	4.45	0.9	0.12	5.361	0.721	
HD184768	5713	94	3.9	4.3	0.9	0.00	4.590	0.643	
HD185144	5271	79	6.3	4.2	1.1	-0.28	5.857	0.786	
HD186039	6074	43	9.8	4.2	1.1	-0.12	4.026	0.510	
HD186104	5753	95	5.8	4.2	1.1	0.10	4.616	0.617	
HD186379	5941	67	9.8	4.0	1.2	-0.31	3.602	0.519	
HD186408	5803	83	3.1	4.2	1.1	0.14	4.304	0.619	
HD186427	5752	77	3.5	4.2	1.1	0.07	4.581	0.632	
HD187123	5824	86	5.0	4.4	0.9	0.15	4.438	0.612	
HD187691	6095	7	29.1	4.2	1.3	0.18	3.688	0.514	
HD187897	5887	95	5.0	4.3	1.1	0.13	4.528	0.597	
HD189087	5341	83	4.0	4.4	1.1	-0.07	5.849	0.778	
HD189340	5816	90	8.4	4.1	1.2	-0.15	3.927	0.556	
HD190067	5387	100	10.3	4.2	1.1	-0.36	5.713	0.696	
HD191785	5212	75	5.8	4.3	0.9	-0.11	5.774	0.822	
HD195005	6075	51	6.7	4.2	1.3	-0.01	4.302	0.498	
HD195104	6103	28	11.3	4.3	1.1	-0.14	4.254	0.464	
HD196218	6115	32	15.3	4.0	1.35	-0.16	3.909	0.441	
HD197076	5821	75	5.6	4.3	1.2	-0.12	4.826	0.592	
HD199960	5878	78	5.9	4.2	1.1	0.28	4.100	0.600	
HD200560	5065	85	5.0	4.3	1.1	0.10	6.241	0.961	
HD200790	6118	8	34.0	4.0	1.55	0.04	3.117	0.486	
HD202108	5712	82	7.2	4.4	0.9	-0.15	5.180	0.617	
HD203235	6071	52	8.4	4.1	1.1	0.10	3.450	0.490	
HD205702	6020	50	4.7	4.2	1.1	0.06	3.843	0.510	
HD206374	5622	89	5.4	4.5	0.5	0.03	5.300	0.665	
HD207795	5323	93	5.8	4.5	0.8	0.13	5.886	0.820	
HD208313	5075	72	5.3	4.3	1.1	-0.10	6.178	0.919	
HD209965	6008	57	8.4	4.2	1.1	-0.17	3.016	0.519	
HD210667	5461	81	5.6	4.5	0.9	0.20	5.465	0.791	
HD210752	6014	70	13.0	4.6	1.1	-0.48	4.568	0.501	
HD211472	5319	91	5.3	4.4	1.1	0.01	5.838	0.796	
HD215065	5726	95	9.7	4.3	0.9	-0.39	5.130	0.597	

Table 1 (Continued)

Star	T_{eff} , K	N	σ , K	$\log g$	V_t , km s^{-1}	[Fe/H]	M_V	(B-V)	Remarks
HD215704	5418	95	4.9	4.2	1.1	0.12	5.492	0.789	
HD217014	5778	92	5.4	4.2	1.1	0.19	4.523	0.632	
HD218209	5705	66	8.1	4.5	1.0	-0.38	5.124	0.611	
HD218868	5554	91	5.8	4.3	1.0	0.23	5.127	0.736	
HD219134	4900	63	7.9	4.2	0.8	0.10	6.468	0.995	
HD220182	5372	94	4.7	4.4	1.2	-0.01	5.650	0.779	
HD221354	5295	95	5.5	4.3	0.8	0.11	5.614	0.819	
HD221851	5181	78	4.9	4.3	1.2	-0.12	6.047	0.851	
HD222143	5799	105	3.6	4.4	1.0	0.11	4.768	0.615	
HD224465	5761	105	3.3	4.4	1.0	0.08	4.814	0.647	
BD+32 1561	4950	82	6.2	4.0	1.3	-0.22	6.480	0.942	
Sun	5777	889	0.9	4.5	0.8	0.05			